AGU PUBLICATIONS

Geophysical Research Letters

RESEARCH LETTER
10.1002/2016GL067938

Key Points:
- Hiss, lightning-generated whistlers, and VLF transmitters can cause butterfly distributions at $L = 2$
- Cross diffusion and boundary conditions must be treated properly to reproduce the distributions
- The butterfly distributions may be enhanced by magnetosonic waves

Correspondence to:
J. M. Albert,
jay.albert@us.af.mil

Citation:
Albert, J. M., M. J. Starks, R. B. Horne, N. P. Meredith, and S. A. Glauert (2016), Quasi-linear simulations of inner radiation belt electron pitch angle and energy distributions, *Geophys. Res. Lett.*, *43*, 2381–2388, doi:10.1002/2016GL067938.

Received 22 JAN 2016
Accepted 1 MAR 2016
Accepted article online 6 MAR 2016
Published online 24 MAR 2016

Quasi-linear simulations of inner radiation belt electron pitch angle and energy distributions

Jay M. Albert[1], Michael J. Starks[1], Richard B. Horne[2], Nigel P. Meredith[2], and Sarah A. Glauert[2]

[1] Air Force Research Laboratory, Kirtland AFB, Albuquerque, New Mexico, USA, [2] British Antarctic Survey, Cambridge, UK

Abstract "Peculiar" or "butterfly" electron pitch angle distributions (PADs), with minima near 90°, have recently been observed in the inner radiation belt. These electrons are traditionally treated by pure pitch angle diffusion, driven by plasmaspheric hiss, lightning-generated whistlers, and VLF transmitter signals. Since this leads to monotonic PADs, energy diffusion by magnetosonic waves has been proposed to account for the observations. We show that the observed PADs arise readily from two-dimensional diffusion at $L = 2$, with or without magnetosonic waves. It is necessary to include cross diffusion, which accounts for the relationship between pitch angle and energy changes. The distribution of flux with energy is also in good agreement with observations between 200 keV and 1 MeV, dropping to very low levels at higher energy. Thus, at this location radial diffusion may be negligible at subrelativistic as well as ultrarelativistic energy.

1. Introduction

"Peculiar" electron pitch angle distributions (PADs) in the inner radiation belt and slot region, with minima near 90°, were recently described by *Zhao et al.* [2014a, 2014b]. These observations were made between September 2012 and March 2014 by the MagEIS instrument on board the Van Allen Probes satellites, which suffers far less from proton contamination than previous instruments. These PADs occurred often over the 200 keV to 1 MeV energy range of the MagEIS medium-energy spectrometer, at L values from 1 to 4. At $E = 460$ keV, they are reported to dominate and persist for $L \sim 1.4–1.8$ and dominate at $L = 1.8–3.5$ during injections but gradually decay during quiet times. Overall, their occurrence rate between $L = 1.5$ and 3 was found to be 61%.

Several possible mechanisms were considered, particularly local heating by chorus or magnetosonic (MS) waves, similar to what is believed to occur in the outer radiation belt [*Albert*, 2005; *Glauert and Horne*, 2005]. MS waves, like chorus, can drive energy diffusion preferentially at intermediate pitch angles [*Horne et al.*, 2007]. Unlike chorus, MS waves are found both inside and outside the plasmasphere and so are a more plausible candidate at $L = 2$. Plasmaspheric hiss was discussed but only as a driver of pitch angle scattering, which is a traditional but, as we show, incomplete perspective.

In this paper, we present two-dimensional quasi-linear diffusion simulations at $L = 2$. Using realistic wave models, with or without magnetosonic waves, we find that the observed peculiar PADs arise readily as long as cross diffusion, which accounts for the relationship between pitch angle and energy changes, is properly included. The distribution of flux with energy is also examined and found to be in good agreement with observations between 200 keV and 1 MeV, dropping to very low levels at higher energy.

2. Waves and Diffusion Rates

Local quasi-linear diffusion coefficients describe diffusion in pitch angle α and momentum p, caused by interactions with waves that satisfy the resonance condition, $\omega - k_{\|} v_{\|} = s n \Omega_c / \gamma$, for some integer n. (Here s is the sign of the particle charge, -1 for electrons, while the nonrelativistic particle gyrofrequency Ω_c is unsigned; the pitch angle is given by $\cos\alpha = v_{\|}/v$, and the wave normal angle is given by $\cos\theta = k_{\|}/k$.) As defined by *Lyons* [1974] and *Albert* [2005], these diffusion coefficients all have dimensions p^2/t and are related by

$$\frac{D_{\alpha p}}{D_{\alpha\alpha}} = \frac{\sin\alpha\cos\alpha}{-\sin^2\alpha + s n \Omega_c/\omega\gamma}, \quad \frac{D_{pp}}{D_{\alpha\alpha}} = \left(\frac{D_{\alpha p}}{D_{\alpha\alpha}}\right)^2 \tag{1}$$

for each value of n.

In the inner magnetosphere, and especially within the high-density plasmasphere, energetic electrons are typically resonant with wave frequencies small compared to Ω_c. Thus, if cyclotron resonances, with $n \neq 0$, occur, $D_{pp}/D_{\alpha\alpha} \sim \omega^2/\Omega_c^2 \ll 1$ and for some purposes diffusion in p (or equivalently, in energy E) may be neglected. This simplification is the traditional basis for treating the interaction of radiation belt electrons with whistler mode hiss as pure pitch angle diffusion [e.g., *Lyons et al.*, 1972], leading to simple exponential decay [e.g., *Lyons and Thorne*, 1973]. However, cyclotron resonance is frequently restricted to values of equatorial pitch angle α_0 well below 90°. Equation (37) of *Albert* [1999] gives an upper bound on such values of α_0, which is reduced for lower density (ω_{pe}/Ω_e), lower wave frequency (ω/Ω_e), higher wave normal angle θ, and lower particle energy.

It has long been recognized that the Landau resonance $n = 0$ makes an essential contribution for particles with moderately large values of equatorial pitch angle α_0. However, since for plasmaspheric hiss the refractive index is large ($kc/\omega \gg 1$), Landau resonance requires small values of $\cos\theta \cos\alpha$. Thus, for quasi-field-aligned waves Landau resonance requires large values of α, so that $D_{pp}/D_{\alpha\alpha} \sim 1/\tan^2\alpha$ is still small for large α. However, the effects of energy diffusion within the plasmasphere have not been thoroughly investigated.

This situation is somewhat different for magnetosonic (MS) waves. Because MS waves are highly oblique (small values of $\cos\theta$), Landau resonance does not require small values of $\cos\alpha$, and energy diffusion relative to pitch angle diffusion need not be small. In this study, MS waves will also be treated with quasi-linear theory, ignoring effects of transit time scattering [*Bortnik and Thorne*, 2010; *Bortnik et al.*, 2015; *Li et al.*, 2014] and bounce resonance [*Chen et al.*, 2015].

Because resonant changes in pitch angle and energy are not independent, combining pitch angle and energy diffusion also requires consideration of their coupling, described by the cross-diffusion coefficient $D_{\alpha p}$. This effect has been shown to be significant in studies of interactions with chorus waves outside the plasmasphere [e.g., *Albert and Young*, 2005; *Tao et al.*, 2008; *Albert et al.*, 2009; *Subbotin et al.*, 2010; *Xiao et al.*, 2010]. In fact, *Tao et al.* [2009] included cross diffusion in a "layer" method applied to MS waves combined with a model of plume hiss and, separately, to chorus waves at $L = 4.5$.

2.1. Wave Models

To quantitatively assess the effects of these interactions, detailed wave models are required. We use models of plasmaspheric hiss, lightning-generated whistlers (LGWs), and waves from ground-based very low frequency (VLF) transmitters [*Abel and Thorne*, 1998] and consider the additional effects of magnetosonic waves.

Hiss and LGW were combined in a recently developed empirical model [*Glauert et al.*, 2014], which follows the procedure of *Meredith et al.* [2004, 2007, 2009]. Electric field spectral intensities measured by the CRRES satellite were converted to magnetic spectral intensities, fit in adjacent frequency ranges by Gaussians, and supplemented by wave normal angle distributions derived from ray tracing. The maximum value of the *AE* index over the previous 3 h, denoted by AE^*, was considered in three different ranges (quiet: <100 nT, moderate: $100 < AE^* < 300$, and active: >300 nT) to generate the spectral intensities and corresponding drift-averaged diffusion coefficients at $L = 2.0, 2.5, \ldots, 6.5$. Dependence on the cold electron density, or the ratio f_{pe}/f_{ce}, is implicitly included in the parameterization by AE^* and not treated as an independent quantity.

The most powerful, currently operating VLF transmitters were individually modeled in detail using the 3-D ray and power tracing described by *Starks et al.* [2008]; this code tracks wave amplitudes as well as wave paths and wave normal angles. Initial amplitudes in the plasmasphere were set accounting for recent advances in modeling transionospheric attenuation, based on full-wave simulation [*Cohen et al.*, 2012; *Graf et al.*, 2013]. The resulting distributions of narrowband waves were used to construct drift-averaged diffusion coefficients following *Albert* [2010], which were further averaged over local time. This procedure was repeated using both the "high-" and "low-" density models shown in Figure 2 of Starks et al. Within the plasmasphere and above $L = 1.2$, these are given roughly by $n_e = 3880(L-1)^{-1.68}$ cm^{-3} and $1350(L-1)^{-1.48}$ cm^{-3}, respectively. Further details of the transmitter modeling will be given in future work.

Magnetosonic waves were considered by *Meredith et al.* [2008, 2009], but the magnetic spectral intensity was an order of magnitude lower than that for hiss under quiet conditions, with correspondingly small diffusion coefficients. On the other hand, *Horne et al.* [2007] analyzed an observation by the Cluster 3 satellite of magnetosonic waves at $L = 4.5$, outside the plasmasphere, that were determined to have much larger magnetic field amplitude, namely, 218 pT. A recent study by *Xiao et al.* [2015] reported a magnetosonic wave

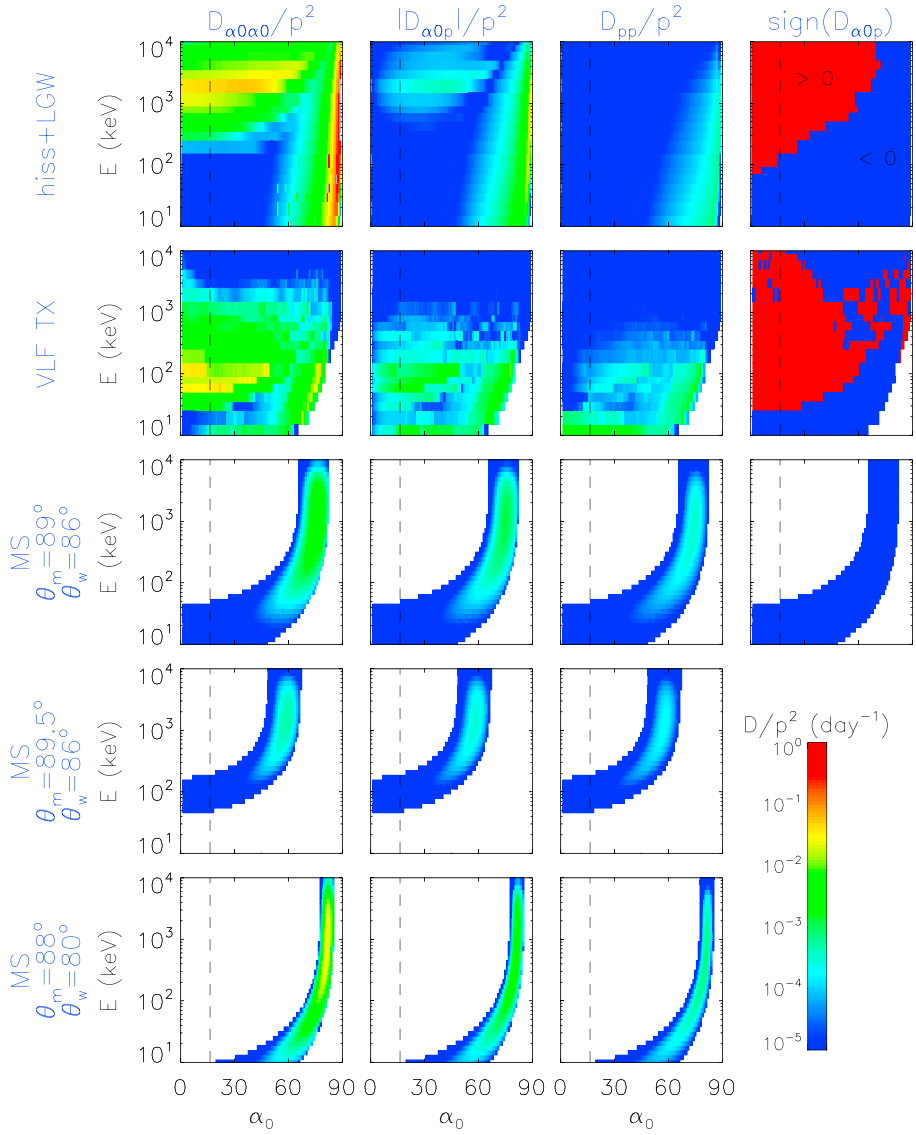

Figure 1. Bounce-averaged quasi-linear diffusion coefficients at $L = 2$ in units of d^{-1}, as functions of equatorial pitch angle α_0 and energy. (first row) Hiss and lightning-generated whistlers (moderate AE^*). (second row) Ground-based VLF transmitters (high-density model). (third to fifth rows) Magnetosonic waves, also for the high-density model, with several different wave normal angle models. The vertical dashed lines mark the edge of the loss cone.

measurement by Van Allen Probe A at $L = 3$ with amplitude 261 pT during a geomagnetic storm on 29 July 2013. This was used in combination with chorus waves to reproduce a butterfly pitch angle distribution observed at $L = 4.8$, i.e., outside the plasmasphere.

A statistical survey of Time History of Events and Macroscale Interactions during Substorms (THEMIS) data by *Ma et al.* [2013] suggested an RMS amplitude outside the plasmapause of 50 pT, with an occurrence rate of 20%, under disturbed conditions (AE^* >300 nT), and smaller values under quieter conditions. They also suggested that the peak frequency scales with the local equatorial gyrofrequency outside the plasmapause but is relatively constant inside. These findings were confirmed by a more recent, similar study of Van Allen Probes measurements [*Ma et al.*, 2015], which reported MS wave amplitude within the plasmasphere of 50 pT near the duskside when AE^* >300 nT, with considerably weaker waves at other magnetic local time sectors, or under less disturbed conditions. Using these indications to modify the model of *Horne et al.* [2007], we adopt the following values for magnetosonic waves at $L = 2$: $B_w^2 = 50^2 \times 0.20 = 500$ pT^2, $\omega_m = 3.49 \times 10^{-3}\ \Omega_{PP}$, $\delta\omega = 8.86 \times 10^{-4}\ \Omega_{PP}$, with cutoffs $\omega_{LC} = \omega_m - 1.5\delta\omega$ and $\omega_{UC} = \omega_m + 2\delta\omega$. Here Ω_{PP} is the value of the electron

gyrofrequency at the plasmapause, which is taken to be at $L = 3$. These frequencies may also be expressed in terms of the lower hybrid frequency at the plasmapause, i.e., $\omega_m = 0.15\,\omega_{LH}$, $\delta\omega = 0.038\,\omega_{LH}$. According to this prescription, setting the plasmapause at a larger value of L would give lower wave frequencies at $L = 2$, resulting in lower diffusion rates; with the plasmasphere at $L = 4.5$, the computed MS diffusion coefficients are smaller by about an order of magntitude. The frequencies reported by *Xiao et al.* [2015] are lower by about a factor of 2, relative to the local gyrofrequency, than those found by *Horne et al.* [2007] and would similarly result in lower diffusion rates, assuming all other parameters are unchanged.

For the distribution of wave normal angles, we follow previous studies [*Horne et al.*, 2007; *Bortnik and Thorne*, 2010; *Xiao et al.*, 2015; *Ma et al.*, 2015] in assuming a Gaussian distribution in $x = \tan\theta$, with peak $x_m = \tan 89°$, width $x_w = \tan 86°$, and cutoffs $x_{min} = x_m - 2x_w$ and $x_{max} = x_m + 2x_w$. These very oblique angles are generally consistent with studies of linear growth rates and particle-in-cell simulations [e.g., *Horne et al.*, 2000; *Ma et al.*, 2013; *Min and Liu*, 2015]. Decreasing the values used was found to cause the peak values of the diffusion coefficients to increase but occur at larger pitch angles, over a narrower range, while increasing them had the opposite effect. The resulting simulations of particle flux, however, were qualitatively unchanged. The MS waves are restricted to within 3° of the equator. Finally, the cold electron density was taken from the high and low models mentioned above, which give values of $f_{pe}/f_{ce} = 4.98$ and 2.94, respectively, at $L = 2$. The high-density model gives larger peak values of the diffusion coefficients, at larger pitch angles but over a narrower range, consistent with the calculations of *Horne et al.* [2007] and *Albert* [2008].

2.2. Diffusion Coefficients

Figure 1 shows the resulting diffusion coefficients at $L = 2$ for $E = 10$ keV to 10 MeV, using the moderate AE^* version of the hiss+LGW model and the high-density versions of the VLF and MS models. The hiss+LGW values at large values of α_0 are due to Landau resonance, and above a few hundred keV, cyclotron resonance contributes to pitch angle diffusion at lower values of α_0, with a familiar deep minimum in between. Energy diffusion (D_{pp}) and cross diffusion ($D_{\alpha_0 p}$) mostly come only from Landau resonance and are much smaller. As expected, diffusion by MS waves comes only from Landau resonance and the three rates are comparable in magnitude; also, $D_{\alpha_0 p}$ for MS waves is always negative. The largest MS pitch angle diffusion rates can exceed the corresponding values for hiss+LGW, and the MS energy diffusion rate is also competitive, over a restricted range of equatorial pitch angle. The effects of changing from the default wave normal angle model for MS waves ($x_m = \tan 89°$ and $x_w = \tan 86°$) to larger values ($x_m = \tan 89.5°$ and $x_w = \tan 86°$) or smaller values ($x_m = \tan 88°$ and $x_w = \tan 80°$), mentioned above, are also shown.

It is a well-known issue in quasi-linear theory that the resonance condition becomes difficult to satisfy for nearly equatorially mirroring particles. However, the hiss+LGW model has nonzero diffusion through $\alpha_0 = 89°$, which for modeling purposes will be considered equivalent to 90°.

3. Simulations

In terms of $x = \alpha_0$ and $y = \log(p/mc)$, the bounce-averaged two-dimensional diffusion equation may be written as

$$\frac{\partial f}{\partial t} = \frac{1}{Gp}\frac{\partial}{\partial x}\left[Gp\left(D_{xx}\frac{\partial f}{\partial x} + D_{xy}\frac{\partial f}{\partial y}\right)\right] + \frac{1}{Gp}\frac{\partial}{\partial y}\left[Gp\left(D_{xy}\frac{\partial f}{\partial x} + D_{yy}\frac{\partial f}{\partial y}\right)\right], \tag{2}$$

where G is the usual (α_0, p) Jacobian factor $p^2 T(\alpha_0)\sin\alpha_0\cos\alpha_0$ [*Schulz and Lanzerotti*, 1974]. These diffusion coefficients are related to those of *Lyons* [1974] by $[D_{xx}, D_{xy}, D_{yy}] = [D_{\alpha_0\alpha_0}, D_{\alpha_0 p}, D_{pp}]/p^2$ and have dimension $1/t$.

Several numerical schemes have been advanced for solving equation (2), including algorithms based directly or indirectly on stochastic differential equations [*Tao et al.*, 2008, 2009]. The merits and shortcomings of several grid-based finite difference schemes were discussed at length by *Camporeale et al.* [2013a, 2013b, 2013c] and *Albert* [2013], and one conclusion is that most such schemes are not guaranteed to maintain positive values of the solution f, though this occurrence may be postponed at the cost of high spatial resolution. The simulations presented here use the scheme of *Albert and Young* [2005], which "diagonalizes" equation (2) by constructing modified coordinates (Q_1, Q_2), with $Q_1 = x$ and $Q_2 \approx y$, that transform away the troublesome cross terms. In these variables, it is feasible to use a relatively coarse grid: 83 values of Q_1 (at integer values between 16° and 89°) and 50 values of Q_2. The time step was taken to be one fourth of the maximum allowed by the

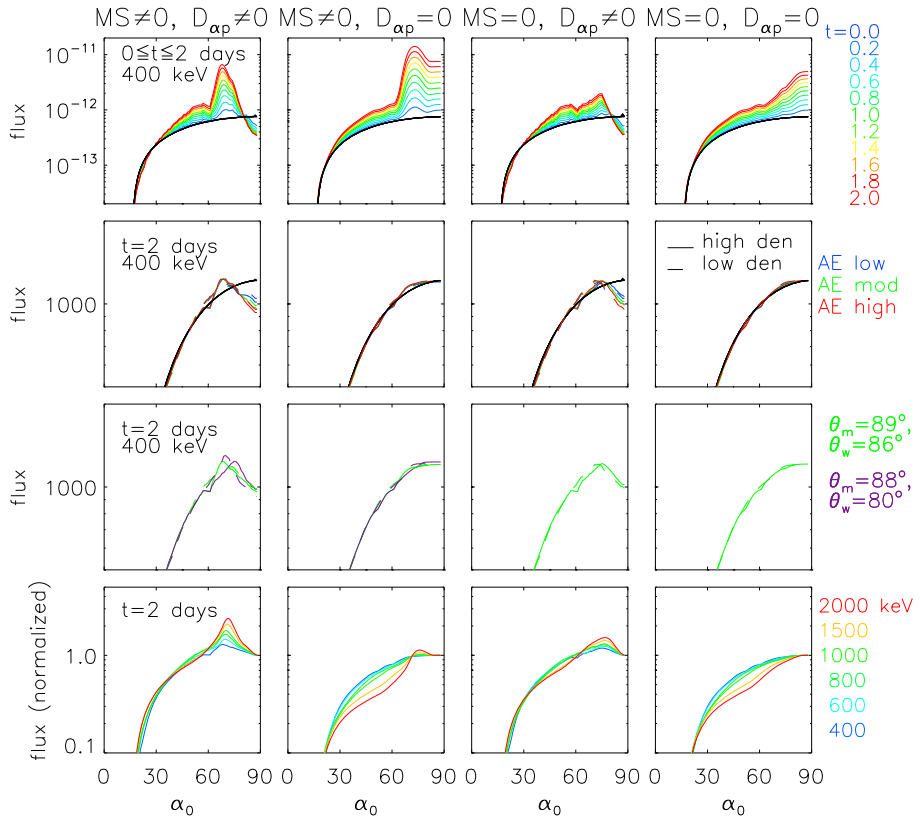

Figure 2. Pitch angle distributions at $L = 2$. (first column) Includes both MS waves and cross diffusion. (second column) Includes MS waves but omits cross diffusion. (third column) Includes cross diffusion but omits MS waves. (fourth column) Omits both MS waves and cross diffusion. Fluxes are given in cm^{-2} s^{-1} sr^{-1} keV^{-1}. (first row) Time development of flux at $E = 400$ keV over 2 days, starting from very low levels (shown by the black curve), using the moderate AE^* hiss+LGW model and high-density VLF and MS models. (second row) Flux at $E = 400$ keV after 2 days, starting from more typical values (shown by the black curve), using six combinations of wave models (corresponding to three ranges of AE^* and two density models, as indicated). For MS waves, $\theta_m = 89$ $\theta_w = 86°$ was used. (third row) Flux at $E = 400$ keV after 2 days for moderate AE^*, using the high- and low-density models and two different versions of the MS wave normal angle models, as indicated. (fourth row) Normalized flux after 2 days, using the wave models of Figure 2 (first row), for several values of E.

Courant-Friedrichs-Lewy stability criterion, and ranged from 6.5 s to 13 s, depending on the wave models used. As a check, some simulations were also done using a straightforward finite difference scheme in (x, y) coordinates, which required a much finer, 400 × 400 grid. For those runs, the maximum time step allowed by stability ranged from 0.5 s to 1.2 s; the value used was 0.17 s.

The domain was taken to be rectangular in the variables used, with fixed values at the low-energy (y or Q_2) boundary corresponding to 200 keV, $f = 0$ at the high-energy (y or Q_2) boundary corresponding to 5 MeV, $f = 0$ at the loss cone (low x or Q_1), and zero transport across the high x (or Q_1) grid boundary, which corresponds to equatorially mirroring particles. In the (Q_1, Q_2) simulations this last boundary condition is simply $\partial f/\partial Q_1 = 0$, but in (x, y) it takes the form

$$D_{xx}\frac{\partial f}{\partial x} + D_{xy}\frac{\partial f}{\partial y} = 0, \tag{3}$$

as discussed by *Zheng et al.* [2014], rather than the simpler constraint $\partial f/\partial x = 0$. The initial condition was chosen to have the simple form $f = j/p^2$ with flux

$$j = j_0 e^{-E/E0}\left(\sin\alpha_0 - \sin\alpha_{LC}\right), \tag{4}$$

where α_{LC} is the loss cone value of α_0 in a dipole field. The constant was set to $j_0 = 2.5\times10^5$ cm^{-2} s^{-1} sr^{-1} keV^{-1}, roughly consistent with the recent observations of *Fennell et al.* [2015], and the values at the low-energy boundary were held fixed.

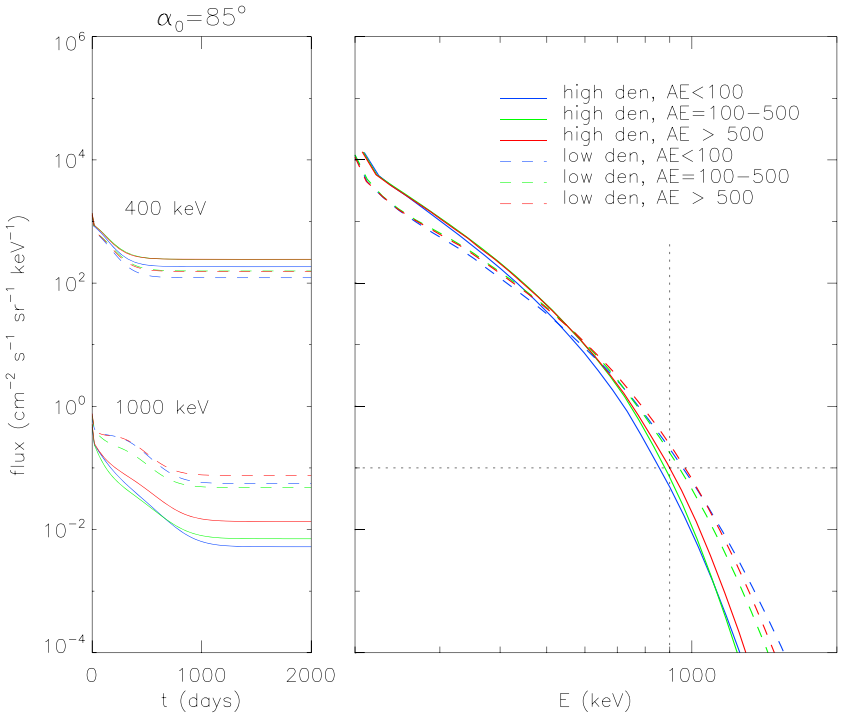

Figure 3. Numerical results at $L = 2$ after 2000 days of simulated time. (left) The simulations have all reached steady state. (right) Energy distributions for $\alpha_0 = 85°$, for different six combinations of wave models. The observed threshold value of 0.1 cm^{-2} s^{-1} sr^{-1} keV^{-1} at 900 keV is marked.

Figure 2 (first row) shows results for 400 keV electrons starting with initial conditions given by equation (4) with $E_0 = 10$ keV; this very steep initial falloff with E is unrealistic but instructive. Because of the steep gradients, this case was too demanding for a straightforward simulation in (x, y) so was only done using the (Q_1, Q_2) diagonalization algorithm. The time development over 2 days is shown in color, using the moderate AE^* range of the hiss+LGW model and the high-density transmitter wave model. The peaked pitch angle distributions develop almost immediately in the runs including cross diffusion, either with magnetosonic waves (first column) or without them (third column). With magnetosonic waves but without cross diffusion (second column) a less drastic peak develops but gradually fades after several days (not shown). Omitting both magnetosonic waves and cross diffusion (fourth column) only gives monotonic pitch angle distributions at all times. Similar behavior was seen in a two-dimensional study of 2 MeV electrons at $L = 4.5$ acted on by magnetosonic waves combined with plume hiss [*Tao et al.*, 2009, Figure 8] and also in a two-dimensional study of MeV electrons at $L = 4.5$ acted on by chorus waves [*Albert and Young*, 2005].

Figure 2 (second row) shows the results for 400 keV electrons starting from the initial conditions of equation (4) with the more realistic value $E_0 = 80$ keV, after 2 days of simulated time. The first column, which includes magnetosonic waves, exhibits clear dips between values at $\alpha_0 = 60°$ and 90°. (The initial, monotonic profile is shown in black.) Curves for each of the six combinations of hiss+LGW and transmitter models are shown as solid and dashed blue, green, and red curves, but there is surprisingly little variation on this timescale. The second column shows results obtained by neglecting cross diffusion: only monotonic profiles are obtained, despite the off-equatorial heating by MS waves. The third column shows that omitting the MS waves but retaining cross diffusion also results in peaked profiles. Omitting both MS waves and cross diffusion, as shown in the fourth column, also gives monotonic profiles. Similar results were also obtained at $L = 2.5$ (not shown). These results were all obtained using the (Q_1, Q_2) algorithm, but they were also checked by simple, direct simulation in (x, y), using a much finer grid as discussed above. The third row repeats the results for moderate AE^* (green curves) and also shows results with the MS wave normal angles changed to $\theta_m = 88$ and $\theta_w = 80$ (purple curves). The changes are very small.

Figure 2 (fourth row) shows normalized pitch angle distributions for several different values of energy, after 2 days, using the hiss+LGW model at the moderate AE^* range and the high-density version of the transmitter

wave model. At each energy, peaked pitch angle distributions are obtained if and only if cross diffusion is included, though they are enhanced by the presence of magnetosonic waves.

The two-dimensional simulations also provide profiles of flux as a function of energy. Figure 3 shows results at $L = 2$ for $\alpha_0 = 85°$, including both magnetosonic waves and cross diffusion, after 2000 days. Figure 3 (left) shows that steady state has been reached well before this. Figure 3 (right) gives the energy profiles for the six combinations of wave models. It might be anticipated that the energy diffusion rates shown in Figure 1, especially for magnetosonic waves, would produce substantial flux levels at several MeV. However, the numerical results show extremely low fluxes above 900 keV, in good qualitative agreement with the recent observations of *Fennell et al.* [2015, Figure 2a]. The reported upper limit of 0.1 $cm^{-2}s^{-1}$ sr^{-1} keV^{-1} at 900 keV is indicated.

4. Summary and Discussion

Two-dimensional simulations of quasi-linear diffusion at $L = 2$ have been performed, using several versions of recently developed, realistic models of plasmaspheric hiss, lightning-generated whistlers, and ground VLF transmitter signals and a somewhat more idealized model of magnetosonic waves. All six versions of the wave models (three AE^*-dependent levels of hiss+LGW, combined with low- or high-density versions of the VLF and MS models) produce pitch angle distributions peaked at 60°–70°, like those recently observed, within a day provided that pitch angle, energy, and cross diffusion (and the corresponding boundary condition at 90°) are properly accounted for. The behavior is caused by strong energy and cross diffusion at large pitch angle, associated with Landau resonance ($n = 0$). Diffusion by magnetosonic waves also has these characteristics and contributes to the size and promptness of the effect but, as modeled, do not seem to be the dominant cause. This conclusion seems robust to changes in the MS wave model parameters, in particular the wave normal angle distributions, though further exploration is called for.

The question arises of how to account for "normal" or "capped" (90° peaked) pitch angle distributions, which together occur between $L = 1.5$ and 3 about 37% of the time [*Zhao et al.*, 2014b]. These may be due to waves differing from the models used. For example, the energy diffusion (and cross diffusion) provided by the hiss+LGW model is mostly attributable to Landau resonance dominating cyclotron resonance at intermediate and large pitch angles, which is sensitive to properties of the waves and to the plasmaspheric density [*Albert*, 1999, 2012; *Ripoll et al.*, 2014]. Radial transport, and possible local time effects, also need to be considered.

The energy dependence of electron flux is also predicted by these simulations, and the steady state determined by the scattering and energization rates along with the boundary conditions is in good agreement with recent observations of very low fluxes above about 1 MeV. Conversely, the simulated fluxes below 1 MeV are sufficiently large to account for the observed levels without any input from radial transport. Thus, while it has been suggested that radial transport below $L = 2.8$ is so slow as to constitute a virtual "barrier" to ultrarelativistic electrons [*Baker et al.*, 2014], the results presented here are consistent with a low level of net inward radial transport to $L = 2$ at all energies above 200 keV.

Acknowledgments
J. Albert thanks R.S. Selesick for useful discussions. This work was supported by NASA grant NNG11PJ001 and NASA agreement NNH14AX18I with the Air Force Research Laboratory, the Air Force Office of Scientific Research grant 13RV08COR, and the Natural Environment Research Council.

References

Abel, B., and R. M. Thorne (1998), Electron scattering loss in Earth's inner magnetosphere: 1. Dominant physical processes, *J. Geophys. Res.*, *103*, 2385–2396, doi:10.1029/97JA02919.

Albert, J. M. (1999), Analysis of quasi-linear diffusion coefficients, *J. Geophys. Res.*, *104*, 2429–2441, doi:10.1029/1998JA900113.

Albert, J. M. (2005), Evaluation of quasilinear diffusion coefficients for whistler mode waves in a plasma with arbitrary density ratio, *J. Geophys. Res.*, *110*, A03218, doi:10.1029/2004JA010844.

Albert, J. M. (2008), Efficient approximations of quasi-linear diffusion coefficients in the radiation belts, *J. Geophys. Res.*, *113*, A06208, doi:10.1029/2008JA012936.

Albert, J. M. (2010), Diffusion by one wave and by many waves, *J. Geophys. Res.*, *115*, A00F05, doi:10.1029/2009JA014732.

Albert, J. M. (2012), Dependence of quasi-linear diffusion coefficients on wave parameters, *J. Geophys. Res.*, *117*, A09224, doi:10.1029/2012JA017718.

Albert, J. M. (2013), Comment on "On the numerical simulation of particle dynamics in the radiation belt. Part I: Implicit and semi-implicit schemes" and "On the numerical simulation of particle dynamics in the radiation belt. Part II: Procedure based on the diagonalization of the diffusion tensor" by E. Camporeale et al., *J. Geophys. Res. Space Physics*, *118*, 7762–7764, doi:10.1002/2013JA019126.

Albert, J. M., and S. L. Young (2005), Multidimensional quasi-linear diffusion of radiation belt electrons, *Geophys. Res. Lett.*, *32*, L14110, doi:10.1029/2005GL023191.

Albert, J. M., N. P. Meredith, and R. B. Horne (2009), Three-dimensional diffusion simulation of outer radiation belt electrons during the 9 October 1990 magnetic storm, *J. Geophys. Res.*, *114*, A09214, doi:10.1029/2009JA014336.

Baker, D. N., et al. (2014), An impenetrable barrier to ultrarelativistic electrons in the Van Allen radiation belts, *Nature*, *515*, 531–534, doi:10.1038/nature13956.

Bortnik, J., and R. M. Thorne (2010), Transit time scattering of energetic electrons due to equatorially confined magnetosonic waves, *J. Geophys. Res.*, *115*, A07213, doi:10.1029/2010JA015283.

Bortnik, J., R. M. Thorne, B. Ni, and J. Li (2015), Analytical approximation of transit time scattering due to magnetosonic waves, *Geophys. Res. Lett.*, *42*, 1318–1325, doi:10.1002/2014GL062710.

Camporeale, E., G. L. Delzanno, S. Zaharia, and J. Koller (2013a), On the numerical simulation of particle dynamics in the radiation belt. Part I: Implicit and semi-implicit schemes, *J. Geophys. Res. Space Physics*, *118*, 3463–3475, doi:10.1002/jgra.50293.

Camporeale, E., G. L. Delzanno, S. Zaharia, and J. Koller (2013b), On the numerical simulation of particle dynamics in the radiation belt. Part II: Procedure based on the diagonalization of the diffusion tensor, *J. Geophys. Res. Space Physics*, *118*, 3476–3484, doi:10.1002/jgra.50278.

Camporeale, E., G. L. Delzanno, S. Zaharia, and J. Koller (2013c), Reply to comment by J. M. Albert on "On the numerical simulation of particle dynamics in the radiation belt. Part I: Implicit and semi-implicit schemes" and "On the numerical simulation of particle dynamics in the radiation belt. Part II: Procedure based on the diagonalization of the diffusion tensor", *J. Geophys. Res. Space Physics*, *118*, 7765–7767, doi:10.1002/2013JA019389.

Chen, L., A. Maldonado, J. Bortnik, R. M. Thorne, J. Li, L. Dai, and X. Zhan (2015), Nonlinear bounce resonances between magnetosonic waves and equatorially mirroring electrons, *J. Geophys. Res. Space Physics*, *120*, 6514–6527, doi:10.1002/2015JA021174.

Cohen, M. B., N. G. Lehtinen, and U. S. Inan (2012), Models of ionospheric VLF absorption of powerful ground based transmitters, *Geophys. Res. Lett.*, *39*, L24101, doi:10.1029/2012GL054437.

Fennell, J. F., S. G. Claudepierre, J. B. Blake, T. P. O'Brien, J. H. Clemmons, D. N. Baker, H. E. Spence, and G. D. Reeves (2015), Van Allen Probes show that the inner radiation belt contains no MeV electrons: ECT/MagEIS data, *Geophys. Res. Lett.*, *42*, 1283–1289, doi:10.1002/2014GL062874.

Glauert, S. A., and R. B. Horne (2005), Calculation of pitch angle and energy diffusion coefficients with the PADIE code, *J. Geophys. Res.*, *110*, A04206, doi:10.1029/2004JA010851.

Glauert, S. A., R. B. Horne, and N. P. Meredith (2014), Three-dimensional electron radiation belt simulations using the BAS Radiation Belt Model with new diffusion models for chorus, plasmaspheric hiss, and lightning-generated whistlers, *J. Geophys. Res. Space Physics*, *119*, 268–289, doi:10.1002/2013JA019281.

Graf, K. L., N. G. Lehtinen, M. Spasojevic, M. B. Cohen, R. A. Marshall, and U. S. Inan (2013), Analysis of experimentally validated trans-ionospheric attenuation estimates of VLF signals, *J. Geophys. Res. Space Physics*, *118*, 2708–2720, doi:10.1002/jgra.50228.

Horne, R. B., G. V. Wheeler, and H. Alleyne (2000), Proton and electron heating by radially propagating fast magnetosonic waves, *J. Geophys. Res.*, *5*, 27,597–27,610, doi:10.1029/2000JA000018.

Horne, R. B., R. M. Thorne, S. A. Glauert, N. P. Meredith, D. Pokhotelov, and O. Santolik (2007), Electron acceleration in the Van Allen radiation belts by fast magnetosonic waves, *Geophys. Res. Lett.*, *34*, L17107, doi:10.1029/2007GL030267.

Li, J., et al. (2014), Interactions between magnetosonic waves and radiation belt electrons: Comparisons of quasi-linear calculations with test particle simulations, *Geophys. Res. Lett.*, *41*, 4828–4834, doi:10.1002/2014GL060461.

Lyons, L. R. (1974), Pitch angle and energy diffusion coefficients from resonant interactions with ion-cyclotron and whistler waves, *J. Plasma Phys.*, *12*, 417–432.

Lyons, L. R., and R. M. Thorne (1973), Equilibrium structure of radiation belt electrons, *J. Geophys. Res.*, *78*, 2142–2149, doi:10.1029/JA078i013p02142.

Lyons, L. R., R. M. Thorne, and C. F. Kennel (1972), Pitch-angle diffusion of radiation belt electrons within the plasmasphere, *J. Geophys. Res.*, *77*, 3455–3474, doi:10.1029/JA077i019p03455.

Ma, Q., W. Li, R. M. Thorne, and V. Angelopoulos (2013), Global distribution of equatorial magnetosonic waves observed by THEMIS, *Geophys. Res. Lett.*, *40*, 1895–1901, doi:10.1002/grl.50434.

Ma, Q., W. Li, R. M. Thorne, J. Bortnik, C. A. Kletzing, W. S. Kurth, and G. B. Hospodarsky (2015), Electron scattering by magnetosonic waves in the inner magnetosphere, *J. Geophys. Res. Space Physics*, *121*, 274–285, doi:10.1002/2015JA021992.

Meredith, N. P., R. B. Horne, R. M. Thorne, D. Summers, and R. R. Anderson (2004), Substorm dependence of plasmaspheric hiss, *J. Geophys. Res.*, *109*, A06209, doi:10.1029/2004JA010387.

Meredith, N. P., R. B. Horne, S. A. Glauert, and R. R. Anderson (2007), Slot region electron loss timescales due to plasmaspheric hiss and lightning generated whistlers, *J. Geophys. Res.*, *112*, A08214, doi:10.1029/2006JA012413.

Meredith, N. P., R. B. Horne, and R. R. Anderson (2008), Survey of magnetosonic waves and proton ring distributions in the Earth's inner magnetosphere, *J. Geophys. Res.*, *113*, A06213, doi:10.1029/2007JA012975.

Meredith, N. P., R. B. Horne, S. A. Glauert, D. N. Baker, S. G. Kanekal, and J. M. Albert (2009), Relativistic electron loss timescales in the slot region, *J. Geophys. Res.*, *114*, A03222, doi:10.1029/2008JA013889.

Min, K., and K. Liu (2015), Fast magnetosonic waves driven by shell velocity distributions, *J. Geophys. Res. Space Physics*, *120*, 2739–2753, doi:10.1002/2015JA021041.

Ripoll, J.-F., J. M. Albert, and G. S. Cunningham (2014), Electron lifetimes from narrowband wave-particle interactions within the plasmasphere, *J. Geophys. Res. Space Physics*, *119*, 8858–8880, doi:10.1002/2014JA020217.

Schulz, M., and L. J. Lanzerotti (1974), *Particle Diffusion in the Radiation Belts*, Springer, New York.

Starks, M. J., R. A. Quinn, G. P. Ginet, J. M. Albert, G. S. Sales, B. W. Reinisch, and P. Song (2008), Illumination of the plasmasphere by terrestrial very low frequency transmitters: Model validation, *J. Geophys. Res.*, *113*, A09320, doi:10.1029/2008JA013112.

Subbotin, D., Y. Shprits, and B. Ni (2010), Three-dimensional VERB radiation belt simulations including mixed diffusion, *J. Geophys. Res.*, *115*, A03205, doi:10.1029/2009JA015070.

Tao, X., A. A. Chan, J. M. Albert, and JA. Miller (2008), Stochastic modeling of multidimensional diffusion in the radiation belts, *J. Geophys. Res.*, *113*, A07212, doi:10.1029/2007JA012985.

Tao, X., J. M. Albert, and A. A. Chan (2009), Numerical modeling of multidimensional diffusion in the radiation belts using layer methods, *J. Geophys. Res.*, *114*, A02215, doi:10.1029/2008JA013826.

Xiao, F., Z. Su, H. Zheng, and S. Wang (2010), Three-dimensional simulations of outer radiation belt electron dynamics including cross-diffusion terms, *J. Geophys. Res.*, *115*, A05216, doi:10.1029/2009JA014541.

Xiao, F., C. Yang, Z. Su, Q. Zhou, Z. He, Y. He, D. N. Baker, H. E. Spence, H. O. Funsten, and J. B. Blake (2015), Wave-driven butterfly distribution of Van Allen belt relativistic electrons, *Nat. Commun.*, *6*, 8590, doi:10.1038/ncomms9590.

Zhao, H., X. Li, J. B. Blake, J. F. Fennell, S. G. Claudepierre, D. N. Baker, A. N. Jaynes, D. M. Malaspina, and S. G. Kanekal (2014a), Peculiar pitch angle distribution of relativistic electrons in the inner radiation belt and slot region, *Geophys. Res. Lett.*, *41*, 2250–2257, doi:10.1002/2014GL059725.

Zhao, H., X. Li, J. B. Blake, J. F. Fennell, S. G. Claudepierre, D. N. Baker, A. N. Jaynes, and D. M. Malaspina (2014b), Characteristics of pitch angle distributions of hundreds of keV electrons in the slot region and inner radiation belt, *J. Geophys. Res. Space Physics*, *119*, 9543–9557, doi:10.1002/2014JA020386.

Zheng, L., A. A. Chan, J. M. Albert, S. R. Elkington, J. Koller, R. B. Horne, S. A. Glauert, and N. P. Meredith (2014), Three-dimensional stochastic modeling of radiation belts in adiabatic invariant coordinates, *J. Geophys. Res. Space Physics*, *119*, 7615–7635, doi:10.1002/2014JA020127.